Editors' Suggestion Featured in Physics

# Effect of Strongly Magnetized Electrons and Ions on Heat Flow and Symmetry of Inertial Fusion Implosions

A. Bose,[1,2,*] J. Peebles,[3] C. A. Walsh,[4] J. A. Frenje,[1] N. V. Kabadi,[1] P. J. Adrian,[1] G. D. Sutcliffe,[1] M. Gatu Johnson,[1] C. A. Frank,[2] J. R. Davies,[3] R. Betti,[3] V. Yu. Glebov,[3] F. J. Marshall,[3] S. P. Regan,[3] C. Stoeckl,[3] E. M. Campbell,[3] H. Sio,[4] J. Moody,[4] A. Crilly,[5] B. D. Appelbe,[5] J. P. Chittenden,[5] S. Atzeni,[6] F. Barbato,[6] A. Forte,[6,7] C. K. Li,[1] F. H. Seguin,[1] and R. D. Petrasso[1]

[1]*Plasma Science and Fusion Center, Massachusetts Institute of Technology, Cambridge, Massachusetts, USA*
[2]*Department of Physics and Astronomy, University of Delaware, Newark, Delaware, USA*
[3]*Laboratory for Laser Energetics, University of Rochester, Rochester, New York, USA*
[4]*Lawrence Livermore National Laboratory, Livermore, California, USA*
[5]*Blackett Laboratory, Imperial College, London, United Kingdom*
[6]*Dipartimento SBAI, Universita di Roma La Sapienza, Rome, Italy*
[7]*Department of Physics, University of Oxford, Oxford, United Kingdom*

(Received 16 December 2021; revised 24 February 2022; accepted 31 March 2022; published 11 May 2022)

This Letter presents the first observation on how a strong, 500 kG, externally applied $B$ field increases the mode-two asymmetry in shock-heated inertial fusion implosions. Using a direct-drive implosion with polar illumination and imposed field, we observed that magnetization produces a significant increase in the implosion oblateness (a 2.5× larger $P2$ amplitude in x-ray self-emission images) compared with reference experiments with identical drive but with no field applied. The implosions produce strongly magnetized electrons ($\omega_e \tau_e \gg 1$) and ions ($\omega_i \tau_i > 1$) that, as shown using simulations, restrict the cross field heat flow necessary for lateral distribution of the laser and shock heating from the implosion pole to the waist, causing the enhanced mode-two shape.

DOI: 10.1103/PhysRevLett.128.195002

In inertial confinement fusion (ICF) [1–3], powerful lasers are used to rapidly compress a spherical capsule to reach high central temperatures (> 4 keV) for thermonuclear fusion [4]. If an external magnetic field is applied to ICF implosions [5–7], the field is compressed with the implosion to several times its seed value [8,9]. The field can boost the central temperature by reducing cross field heat losses [10,11], and amplify the fusion self-heating by trapping the charged particles (fusion products) within the hot spot in an ignition experiment [7]. A number of numerical studies [5–7,12,13] and a few experiments [14–16] show the effects of magnetizing an ICF implosion. With recent advances allowing the generation of ever-higher $B$ fields for this purpose [17–22], it is important to experimentally investigate the effect of a strong applied $B$ field on implosions.

Previous magnetized-ICF experiments [14–16] conducted at the OMEGA laser [23] used an initial $B$ field of ≈80 kG externally imposed on plastic capsules. Both cylindrical and spherical capsules were used, with a shell thickness of ≈25 $\mu$m and filled with deuterium ($D$) fuel. These directly driven implosions produced a convergence ratio (CR), i.e., a ratio of capsule initial and final radii, of ≈25×. Considering the $B$ field to be frozen in the $D$ fuel, the initial field is compressed with the implosion $B_f/B_0 = \mathrm{CR}^2 \approx 625\times$, to 30 MG. In the cylindrical experiments, 30–40 MG fields were measured [14], showing good agreement with the frozen-field estimates. In the spherical implosions, the compressed field produced an increase in fusion yield (by 30%) and temperature (by 15%) [15,16]. No discernible difference in implosion shape due to the magnetization was observed in x-ray backlit images [15,16]. It was argued, since the plasma beta ($\beta =$ plasma/magnetic pressure ratio) is typically large ($\approx 10^2$), the applied $B$ field had little or no effect on the implosion shape. However, recent simulation studies [24,25] with a stronger applied $B$ field anticipate an increase in the Rayleigh–Taylor instability growth and shape nonuniformity arising from a suppression in thermal transport caused by magnetization. In this Letter, we report the first experimental results showing how strong applied $B$ fields and subsequently strong plasma magnetization, although at $\beta \gg 1$, affect the shape of directly driven implosions.

The OMEGA laser facility [23] was used to conduct "exploding pusher" [26,27] implosions with a 500 kG seed $B$ field externally imposed on the capsules. A schematic of the experiments is shown in Fig. 1(a). The capsules were spherical shells of 430 $\mu$m outer radius with 2.5 $\mu$m glass walls and filled with a (1 mg/cc) low-density gaseous mixture of DT$^3$He at 1∶9∶10 atomic ratio serving as fusion fuel. The implosions were driven with 40 of the OMEGA laser beams delivering 16.9 kJ energy in a 1 ns duration

 

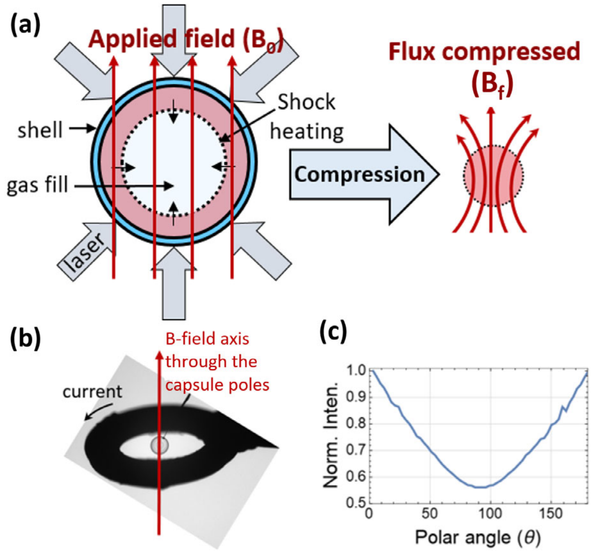


FIG. 1. (a) Schematic of the magnetized implosion experiment, (b) the current carrying coil producing the applied $B$ field, and (c) variation in intensity of laser drive with polar angle.

square pulse. A current carrying coil, shown in Fig. 1(b), attached to MIFEDS [21] was used to produce the applied $B$ field. A nonuniform laser illumination, shown in Fig 1(c), with a relatively higher intensity at the capsule poles than at the waist (a 45% peak-to-valley variation) was used to drive the implosion. The laser drive launches a strong spherically converging shock wave into the capsule. The shock rebounds at the center of the implosion, creating fusion relevant temperatures in the fuel (the measured bang time, yield, and temperature are listed in Table I). The thin glass shell is mostly ablated by the laser. The fuel converges by approximately a factor of $\approx 3\times$ (Table I:c), and the applied $B$ field is compressed with it to a few mega Gauss (Table I:l), producing a fully ionized and magnetized plasma roughly 140 $\mu$m in radius.

Three capsules were shot, two with the $B$ field applied and one reference shot without the field. Table I lists the key experimental results, all inferred from measured quantities. The fuel plasma is highly conductive and has a very large magnetic Reynolds number $\mathrm{Re} > 10^3$ (see Table I:k and table footnotes), similar to Ref. [28]; this implies that the applied $B$ field is frozen in the fuel plasma and compressed to $B_f \approx 3$–5 MG (Table I:l). The compressed field value is validated with resistive magnetohydrodynamic (MHD) simulations (discussed later) and is consistent with previous magnetized-ICF experiments with similar fuel conditions [14]. The large plasma $\beta$ of $\approx 200$ (Table I:m), with values similar to those in Refs. [15,16], imply the magnetic pressure is smaller than the plasma pressure and has no effect on the RTI growth and implosion shape.

In a strongly magnetized plasma the Hall parameter $\chi = \omega\tau = \lambda/r$ is $> 1$, i.e., gyro frequency times collision time $\omega\tau > 1$, or the gyro radius $r$ is shorter than the collision mean-free path $\lambda$. The Hall parameter scales with the observable as $\chi \propto T^{3/2}B/(m^{1/2}n)$. In the experiments, an electron Hall parameter of $\chi_e \approx 50$ and an ion Hall parameter of $\chi_i \approx 7$ (for $D$ and $T$ ions) are inferred (shown in Table I:p). Since the Hall parameter scales with particle mass as $\chi \propto m^{-1/2}$, it is more challenging to magnetize ions over electrons, and ion magnetization has not been demonstrated previously in laser-driven high-energy-density (HED) experiments. However, the spherically converging strong shock in exploding pushers heats the ions to very high temperatures ($T_i \approx 5 \times T_e$ from Table I:f) and since $\chi \propto T^{3/2}$ this platform is capable of producing strongly magnetized ions $\chi_i > 1$ in addition to electrons $\chi_e \gg 1$, which is a salient feature of these experiments. Consequently, the shorter gyro radius $r_{e/i}$ (Table I:n) compared with the collision mean-free path $\lambda_{e/i}$ (Table I:h) limits electron and ion transport perpendicular to the applied $B$ field ($\perp$), which for the ions can be associated with a suppression in ion Knudsen number in the $\perp$ direction $\text{mag-Kn}_\perp/\text{Kn} = \chi_i^{-1} \approx 0.14$ (Table I:j) [26]. However, the transport in the direction $\parallel$ to the $B$ field is unaffected. As a result, the ratio of $\perp$ to $\parallel$ thermal transport is suppressed by $\kappa_\perp/\kappa_\parallel(e) \approx 10^{-4}$ for electrons and $\kappa_\perp/\kappa_\parallel(i) \approx 10^{-2}$ for ions (shown in Table I:q), which can produce a significant directional anisotropy in the heat flow.

The main result is shown in Fig. 2 in the form of x-ray images of the implosions. The images show time-integrated emission taken with the gated monochromatic x-ray imager [29] in the 2–7 keV range, viewing along the implosion waist, i.e., from a polar angle approaching 90°, a view similar to in Fig. 1(c). As illustrated in Fig. 2, the laser heating was higher at the capsule poles than at the waist, with the $B$ field axis running vertically through the center of the images in (b). The darker regions correspond to higher levels of x-ray emission. A comparison between the unmagnetized [Fig. 2(a)] and magnetized [Fig. 2(b)] images show an increased mode-two amplitude when the $B$ field was applied, with a clear correlation between the applied field axis and the mode-two phase. A Legendre polynomial fit to the highlighted contour is used to estimate the average radius of the implosion $P0$ and the amplitude of the dominant mode-two ($P2$) asymmetry. In addition to the 40% of peak intensity contour, the 17% and 30% contours were also used for the analysis; they produced the same mode-two amplitude. The $P2/P0$ ratios are listed in Table I:c. The unmagnetized case produced only a slightly oblate spheroid shaped implosion with a $P2/P0 = -9\%$ and $a/b = 1.115$. The magnetized case produced a significant increase in oblateness with $P2/P0 = -23\%$ for both shots and $a/b = 1.434$ and 1.457 for shots 95292 and 95297 respectively, showing that the field causes the capsule waist to converge less. An increase in oblateness is visible in both the limb brightened outer edge and the

TABLE I. Capsule parameters and resulting key data. Measurements are temporally and spatially averaged over the fuel plasma.

| Shot | $B_o$ (MG) | Capsule[a] OD ($\mu$m) | Capsule[a] Fill and shell (atm) [$\mu$m] | $t_b$[b] $\pm 10$ (ps) | CR[c] $\pm 0.03$ | P2/P0[c] $\pm 1$ (%) | DT-$n$ yield $[Y/Y_{noB}]$[d] | $D^3He-p$ yield $[Y/Y_{noB}]$[d] | $T^3He-d$ yield $[Y/Y_{noB}]$[d] | $T_i$[f] $\pm 0.3$ (keV) | $T_e$[f] $\pm 0.3$ (keV) | $n_i$[g] [D, T, $^3$He] $\times 10^{21}$ (cm$^{-3}$) | $n_e$[g] $\times 10^{21}$ (cm$^{-3}$) |
|---|---|---|---|---|---|---|---|---|---|---|---|---|---|
| 95293 | 0 | 857 | $DT(2.0)^3He(4.6)SiO_2[2.3]$ | 769 | 3.04 | −9 | $2.2 \times 10^{11}$ [1] | $1.3 \times 10^{9}$ [1] | $4.1 \times 10^{8}$ [1] | 11.6 | 2.3 | [0.27, 2.4, 3.1] | 9.0 |
| 95297 | 0.5 | 852 | $DT(2.0)^3He(4.9)SiO_2[2.2]$ | 767 | 2.50 | −23 | $1.6 \times 10^{11}$ [0.77] | $5.1 \times 10^{8}$ [0.43] | $2.0 \times 10^{8}$ [0.55] | 11.6 | 2.2 | [0.16, 1.4, 1.9] | 5.3 |
| 95292 | 0.5 | 888 | $DT(2.1)^3He(4.8)SiO_2[2.4]$ | 827 | 3.13 | −23 | $2.3 \times 10^{11}$ [0.85] | $5.9 \times 10^{8}$ [0.42] | $2.2 \times 10^{8}$ [0.48] | 10.0 | 2.3 | [0.32, 2.8, 3.6] | 10.4 |

| Shot | $\lambda_i$[h] [D, T, $^3$He] $\times 10^2$ ($\mu$m) | $\lambda_e$[h] $\times 10^1$ ($\mu$m) | $Kn$[j] [D, T, $^3$He] | Re[k] $\times 10^3$ | $B_f$[l] (MG) | $\beta$[m] | $r_i$[n] [D, T, $^3$He] $\times 10^1$ ($\mu$m) | $r_e$[n] $\times 10^{-1}$ ($\mu$m) | $mag\text{-}Kn\perp$[j] [D, T, $^3$He] | $\chi_i$[p] [D, T, $^3$He] | $\chi_e$[p] | $\kappa_\perp/\kappa_\parallel(i)$[q] [D, T, $^3$He] $\times 10^{-2}$ | $\kappa_\perp/\kappa_\parallel(e)$[q] $\times 10^{-4}$ |
|---|---|---|---|---|---|---|---|---|---|---|---|---|---|
| 95293 | [2.5, 3.0, 0.8] | 1.2 | [1.8, 2.2, 0.5] | … | … | … | … | … | … | … | … | … | … |
| 95297 | [4.1, 5.0, 1.2] | 1.8 | [2.4, 2.9, 0.7] | 4.4 | 3.1 | 220 | [5.0, 6.1, 3.1] | 3.6 | [0.29, 0.36, 0.18] | [8.3, 8.2, 4.1] | 52 | [1.4, 1.5, 6.0] | 3.8 |
| 95292 | [1.7, 2.0, 0.5] | 1.1 | [1.2, 1.4, 0.4] | 3.1 | 4.9 | 155 | [3.0, 3.6, 1.8] | 2.3 | [0.21, 0.26, 0.13] | [5.6, 5.5, 2.7] | 45 | [3.2, 3.3, 13.2] | 4.8 |

[a]Outer diameter (OD), initial fill-pressure, and shell thickness.
[b]Time of peak DT- $n$ rate.
[c]Implosion convergence (CR) and mode-two amplitude (P2/P0) inferred from x-ray images (in Fig. 2) using the contour at 40% of peak-emission.
[d]Relative yield $[Y/Y_{noB}]$ is the ratio of magnetized to unmagnetized (shot 95293) yield. Shot-to-shot variation arising from small differences in capsule and drive parameters are accounted for by normalizing each measurement with the corresponding 1D yield using *LILAC* (without MHD). Therefore, $[Y/Y_{noB}]$ is the yield difference caused by the applied $B$ field, i.e., taking into account potential yield increase due to magnetization and yield degradation due to the enhanced asymmetry.
[f]Ion and electron temperatures inferred from the measured fusion product energy spectra and x-ray spectra in 4–6 keV range.
[g]Ion [D, T and $^3$He], and electron number density calculated using the CR and initial fill composition.
[h]ion-ion and e-e collision mean-free-paths.
[j]Knudsen number $\equiv \lambda_i/R_f$ and magnetized Knudsen number $\equiv r_i/R_f$.
[k]Magnetic Reynolds number $\equiv t_{diff}/t_b$, where $t_{diff} = 4\pi R_{final}^2/c^2\eta$, with resistivity $\eta$ determined using $T_e$, $Z$ and $\log \lambda_e$.
[l]Final $B$ field $B_f = B_0 CR^{2(1-1/R_m)}$.
[m]plasma beta $\beta = 8\pi nT/B^2$.
[n]Gyro-radii.
[p]Hall parameters.
[q]Thermal conductivity reduction.

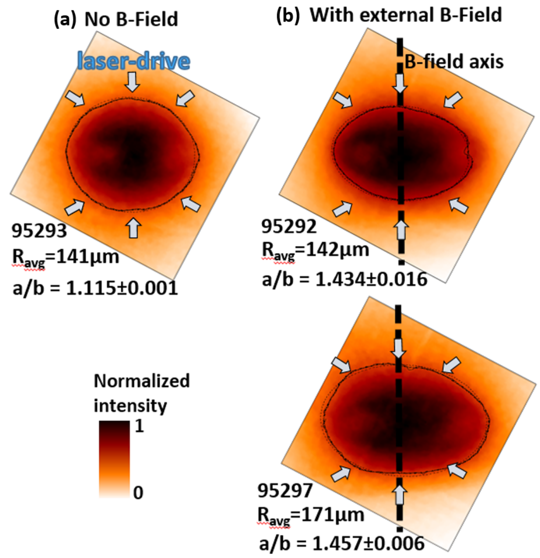


FIG. 2. X-ray self emission images of the (a) unmagnetized and (b) magnetized implosions. The shot number, average radius of the marked contour (corresponding to 40% of peak intensity), and the oblateness parameter $a/b$ (ratio of major-to-minor axis) are listed below each image.

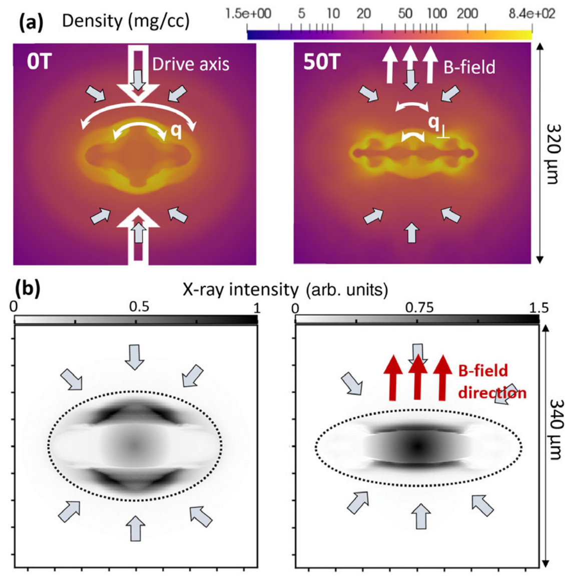


FIG. 3. Density profile at bang time (a), and synthetic x-ray self emission images (b), from simulations with 0 kG (left) and 500 kG (right) applied $B$ field. The shorter curved arrows in (b) represent a reduced cross field heat flow ($q_{\perp}$).

inner regions of the images. Although the laser intensity is 1.8× higher at the pole than at the waist, the relatively round shape for the unmagnetized case suggests that the energy coupled at the pole is conducted laterally to the waist, and for the magnetized case the waist is energy starved. These are the first experimental x-ray images that show a discernible increase in the mode-two asymmetry caused by a strong applied $B$ field.

The magnetized shots exhibit a relative drop in yield compared with the unmagnetized reference shot. The relative yields $[Y,/Y_{\mathrm{no}B}]$ are listed in Table I. Fusion yield for 14.1 MeV DT-neutron, 14.7 MeV D$^3$He-proton, and 9.5 MeV T$^3$He-deuteron all show a degradation in the $[Y,/Y_{\mathrm{no}B}]$, by ≈20%, ≈60%, and ≈50%, respectively. The degradation in yield clearly outweighed any boost in yield arising from the magnetization. The drop in yield with applied $B$ field confirms the conclusion drawn from the x-ray images, that the applied magnetic fields produced an increase in implosion asymmetry.

The following key differences between these and previous magnetized experiments [14–16] facilitated the measurements: (i) The plasma electrons and ions are strongly magnetized with $\chi_e \approx 50$ and $\chi_i \approx 7$ significantly higher than $\chi_e \approx 1$ and $\chi_i \approx 0.01$ in previous experiments [14–16]. The higher magnetization increases the anisotropy in thermal transport. In order to produce strong magnetization, i.e., $\chi \propto T^{3/2}B/(m^{1/2}n) > 1$, a higher initial $B$ field is used (500 kG, versus 80 kG used previously). Since low density and high temperature are favorable for magnetization, exploding pushers are used for their low CR of ≈3×, high $T_i \approx 11$ keV, and $T_e \approx 2$ keV—versus compressive implosions with higher CR ≈ 25×, lower $T_i \approx 2$–4 keV, and comparable $T_e \approx 2$–4 keV—used previously [15,16]. (ii) A nonuniform laser illumination, serving as seed perturbation for $B$-field anisotropy, is used for the ease of low-mode shape measurements. In previous experiments, the laser beams driving the capsule poles were repointed toward the waist [16]. Beam repointing was not applied in these experiments. Finally, (iii) the exploding pusher implosions, by virtue of their low CR, are less susceptible to mid- and short-wavelength background asymmetries [30,31] arising from various extraneous sources that can affect the clarity of x-ray images.

Two-dimensional simulations of these implosions using the extended-MHD code Gorgon [32–34], shown in Fig. 3, also produce an increase in oblateness (or mode-two) due to magnetization with the same mode-two phase with respect to the applied field axis like in the experiments. The $P2/P0$ estimated from simulations with no $B$ field and 500 kG applied field are $\approx -25\%$ and $\approx -63\%$ respectively. This indicates that the magnetization enhances the $P2$ amplitude ≈2.5×, which agrees with the experimental result. The simulations used the same laser illumination pattern as in the experiments and take into account the effect of magnetic pressure and heat-flow suppression due to the magnetization of electrons and ions [35–37]. Although the $B$ field is compressed to mega Gauss levels in the shocked fuel (Fig. 4), simulations show that the plasma beta is large $\beta \approx 10^2$–$10^6 \gg 1$ in the shocked fuel and in the conduction zone. Simulations with the magnetic pressure term turned off in the code show no difference in the implosion shape. Consequently, the magnetic pressure has no effect on the symmetry. The magnetic transport in Gorgon has been

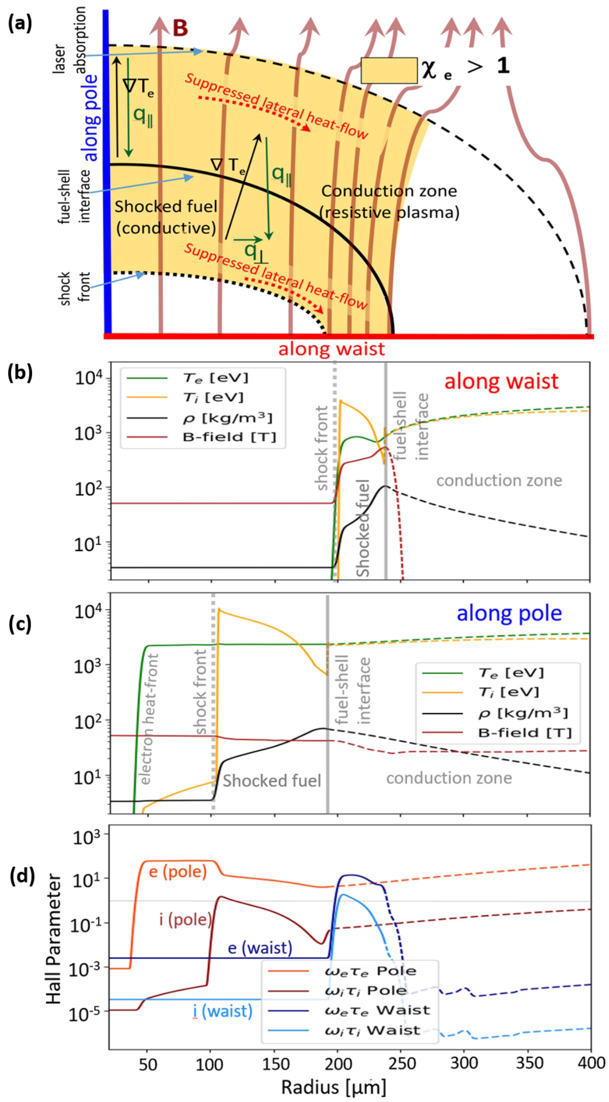


FIG. 4. Magnetized shock-driven implosion at ≈100 ps prior to shock rebound at the center. (a) Illustration showing magnetization ($\chi_e > 1$ using yellow) in the shocked fuel and the conduction zone. The applied $B$-field lines exit near the pole to close outside the implosion. Lineouts from the Gorgon simulation taken along the implosion waist (b) and pole (c). (d) Lineouts showing electron- and Triton- Hall parameters ($\omega_e\tau_e$ and $\omega_i\tau_i$) along the pole and the waist.

benchmarked against magnetic flux compression experiments at OMEGA [38]. The heat flux is given by [24]

$$\vec{q} = -\kappa_{\parallel}\nabla_{\parallel}T_{e/i} - \kappa_{\perp}\nabla_{\perp}T_{e/i} - \kappa_{\wedge}\hat{b}\times\nabla T_{e/i} \qquad (1)$$

where the $\kappa_{\parallel}$ term, representing heat flow parallel to the applied $B$ field, is independent of magnetization [39]. The heat flow perpendicular to the $B$ field is reduced by $\kappa_{\perp} \propto \chi_{e/i}^{-2}$, and the cross gradient (Righi-Leduc) heat flow is reduced by $\kappa_{\wedge} \propto \chi_{e/i}^{-1}$ [37].

The pole-heavy laser drive deposits more energy at the capsule pole and consequently drives a stronger shock at the pole than at the waist. In the unmagnetized case, the lateral heat flow is responsible for distributing the laser and shock heating from the pole to the waist. In the magnetized case, shown in Fig. 4, the lateral heat flow $q_{\perp}$ is suppressed at regions with Hall parameter $\chi > 1$ in the conduction zone and in the shocked fuel, shaded with yellow in (a). A comparison between lineouts taken along the waist [Fig. 4(b)] and along the pole [Fig. 4(c)] shows a lag in the position of the shock front and the electron heat front at the waist. In the shocked-fuel region, the frozen-in $B$ field is compressed to a few mega Gauss which magnetizes the fuel electrons and ions, i.e., $\chi_{e/i} > 1$ [Fig. 4(d)]. Note, since the post-shock ions are significantly hotter than the electrons, the ion heat conduction is not negligible in this region. As a result of magnetization, the $q_{\perp}$ heat flow is restricted, causing the lag in the shock front and electron heat front at the waist (but the $q_{\parallel}$ heat flow is not restricted). The difference in heat flow produces a difference in dynamics between the waist Fig. 4(b) and the pole Fig. 4(c) that increases the mode-two asymmetry in the magnetized case. In addition to the shocked fuel, the conduction zone is also magnetized, as shown by Walsh *et al.* [24]. Although the resistive ablator plasma diffuses the $B$ field out of the conduction zone [at the waist, see Fig. 4(b)], the pole retains the field [see Fig. 4(c)] because the applied $B$ field is normal to the ablator surface. The electrons at the pole are magnetized $\chi_e > 1$ [Fig. 4(d)], and restrict the lateral heat flow to the waist [24], shown in Fig. 4(a). In summary, the increase in mode-two with magnetization is caused by (i) the strongly magnetized electrons and ions in the shocked fuel and (ii) the strongly magnetized conduction zone electrons at the implosion pole. The magnetization at both regions causes an anisotropy in the heat flow between directions $\parallel$ and $\perp$ to the applied $B$ field, essentially suppressing the lateral heat flow responsible for distributing the laser and shock heating from the pole to the waist.

In conclusion, it was shown that imposing strong $B$ fields on shock-heated ICF implosions with a pole-heavy direct-illumination produce an increase in the mode-two shape. Strong magnetization of the electrons and ions restricts the cross field heat flow responsible for the lateral distribution of the laser and shock heating from the pole to the waist. This Letter reports on the first experimental results showing how an applied $B$ field affects the symmetry of ICF implosions. These results motivate future investigations of the correlation between laser-drive uniformity and applied $B$-field strength in strongly magnetized ICF implosions. As magnetization of ICF implosions potentially improves fusion gain, similar studies with a strong applied $B$ field on isentropic compression targets are necessary to identify limits on drive nonuniformity that can be sustained as higher initial magnetic field values and strong magnetization conditions ($\chi_{e,i} \gg 1$) are explored.

This new experimental platform, using a strong $B$ field applied to shock-heated implosions, provides a unique recipe for producing both strongly magnetized ions ($\chi_i > 1$), with an ion Hall parameter comparable to MagLIF implosions [40,41], and electrons ($\chi_e \gg 1$), at high-power laser systems, providing access to strong magnetization regimes with the potential for additional discoveries through future studies on magnetized transport, like thermal conduction and ion viscosity $\propto \chi_i^{-2}$ [42–44], thus, opening avenues for future magnetized HED plasma research.

The work described herein was performed in part by the U.S. Department of Energy (DOE) under Grant No. DE-NA0003868, and at the National Laser Users Facility under Grant No. DE-NA0003938. In addition, during manuscript preparation at the University of Delaware, A. B. and C. F. were supported by the Laboratory for Laser Energetics (LLE), University of Rochester subaward SUB00000056/GR530167/AWD00002510 under DOE Grant No. DE-NA0003856. The work of S. A. and F. B. (Rome) has been supported by EUROfusion under Grant Agreement No. 101052200.

*bose@udel.edu

[1] J. Nuckolls, L. Wood, A. Thiessen, and G. Zimmerman, Laser compression of matter to super-high densities: Thermonuclear (CTR) applications, Nature (London) **239**, 139 (1972).

[2] S. Atzeni and J. Meyer-Ter-Vehn, *The Physics of Inertial Fusion: Beam Plasma Interaction, Hydrodynamics, Hot Dense Matter* (Oxford University Press, Oxford, 2004).

[3] J. D. Lindl, *Inertial Confinement Fusion: The Quest for Ignition and Energy Gain Using Indirect Drive* (Springer, New York, 1998).

[4] J. D. Lawson, Some criteria for a power producing thermonuclear reactor, Proc. Phys. Soc. London Sect. B **70**, 6 (1957).

[5] M. A. Sweeney and A. Farnsworth, High-gain, low-intensity ICF targets for a charged-particle beam fusion driver, Nucl. Fusion **21**, 41 (1981).

[6] I. R. Lindemuth and R. C. Kirkpatrick, Parameter space for magnetized fuel targets in inertial confinement fusion, Nucl. Fusion **23**, 263 (1983).

[7] R. D. Jones and W. C. Mead, The physics of burn in magnetized deuterium-tritium plasmas: Spherical geometry, Nucl. Fusion **26**, 127 (1986).

[8] A. D. Sakharov, Magnetoimplosive generators, Sov. Phys. Usp. **9**, 294 (1966).

[9] F. S. Felber, M. M. Malley, F. J. Wessel, M. K. Matzen, M. A. Palmer, R. B. Spielman, M. A. Liberman, and A. L. Velikovich, Compression of ultrahigh magnetic fields in a gas-puff Z pinch, Phys. Fluids **31**, 2053 (1988).

[10] S. I. Braginskii, Transport processes in a plasma, in *Reviews of Plasma Physics*, edited by M. A. Leontovich (Consultants Bureau, New York, 1965), Vol. I.

[11] R. C. Kirkpatrick, I. R. Lindemuth, and M. S. Ward, Magnetized target fusion: An overview, Fusion Technol. **27**, 201 (1995).

[12] L. J. Perkins, B. G. Logan, G. B. Zimmerman, and C. J. Werner, Two-dimensional simulations of thermonuclear burn in ignition-scale inertial confinement fusion targets under compressed axial magnetic fields, Phys. Plasmas **20**, 072708 (2013).

[13] L. J. Perkins, D. D.-M Ho, B. G. Logan, G. B. Zimmerman, M. A. Rhodes, D. J. Strozzi, D. T. Blackfield, and S. A. Hawkins, The potential of imposed magnetic fields for enhancing ignition probability and fusion energy yield in indirect-drive inertial confinement fusion, Phys. Plasmas **24**, 062708 (2017).

[14] O. V. Gotchev, P. Y. Chang, J. P. Knauer, D. D. Meyerhofer, O. Polomarov, J. Frenje, C. K. Li, M. J.-E. Manuel, R. D. Petrasso, J. R. Rygg, F. H. Séguin, and R. Betti, Laser-Driven Magnetic-Flux Compression in High-Energy-Density Plasmas, Phys. Rev. Lett. **103**, 215004 (2009).

[15] P. Y. Chang, G. Fiksel, M. Hohenberger, J. P. Knauer, R. Betti, F. J. Marshall, D. D. Meyerhofer, F. H. Séguin, and R. D. Petrasso, Fusion Yield Enhancement in Magnetized Laser-Driven Implosions, Phys. Rev. Lett. **107**, 035006 (2011).

[16] M. Hohenberger, P.-Y. Chang, G. Fiksel, J. P. Knauer, R. Betti, F. J. Marshall, D. D. Meyerhofer, F. H. Séguin, and R. D. Petrasso, Inertial confinement fusion implosions with imposed magnetic field compression using the OMEGA Laser, Phys. Plasmas **19**, 056306 (2012).

[17] H. Daido, F. Miki, K. Mima, M. Fujita, K. Sawai, H. Fujita, Y. Kitagawa, S. Nakai, and C. Yamanaka, Generation of a Strong Magnetic Field by an Intense $CO_2$ Laser Pulse, Phys. Rev. Lett. **56**, 846 (1986).

[18] C. Courtois, A. D. Ash, D. M. Chambers, R. A. D. Grundy, and N. C. Woolsey, Creation of a uniform high magnetic-field strength environment for laser-driven experiments, J. Appl. Phys. **98**, 054913 (2005).

[19] S. Fujioka, Z. Zhang, N. Yamamoto *et al.*, High-energy-density plasmas generation on GEKKO-LFEX laser facility for fast-ignition laser fusion studies and laboratory astrophysics, Plasma Phys. Controlled Fusion **54**, 124042 (2012).

[20] S. Fujioka, Z. Zhang, K. Ishihara *et al.*, Kilotesla magnetic field due to a capacitor-coil target driven by high power laser, Sci. Rep. **3**, 1170 (2013).

[21] G. Fiksel, A. Agliata, D. Barnak *et al.*, Experimental platform for magnetized high-energy-density plasma studies at the omega laser facility, Rev. Sci. Instrum. **86**, 016105 (2015).

[22] L. Gao, H. Ji, G. Fiksel, W. Fox, M. Evans, and N. Alfonso, Ultrafast proton radiography of the magnetic fields generated by a laser-driven coil current, Phys. Plasmas **23**, 043106 (2016).

[23] T. R. Boehly *et al.*, Initial performance results of the OMEGA laser system, Opt. Commun. **133**, 495 (1997).

[24] C. A. Walsh, A. J. Crilly, and J. P. Chittenden, Magnetized directly-driven ICF capsules: Increased instability growth from non-uniform laser drive, Nucl. Fusion **60**, 106006 (2020).

[25] C. A. Walsh, K. McGlinchey, J. K. Tong, B. D. Appelbe, A. Crilly, M. F. Zhang, and J. P. Chittenden, Perturbation modifications by pre-magnetisation of inertial confinement fusion implosions, Phys. Plasmas **26**, 022701 (2019).

[26] M. J. Rosenberg, H. G. Rinderknecht, N. M. Hoffman *et al.*, Exploration of the Transition from the Hydrodynamiclike to the Strongly Kinetic Regime in Shock-Driven Implosions, Phys. Rev. Lett. **112**, 185001 (2014).

[27] H. Sio, J. A. Frenje, A. Le *et al.*, Observations of Multiple Nuclear Reaction Histories and Fuel-Ion Species Dynamics in Shock-Driven Inertial Confinement Fusion Implosions, Phys. Rev. Lett. **122**, 035001 (2019).

[28] O. V. Gotchev, N. W. Jang, J. P. Knauer *et al.*, Magneto-inertial approach to direct-drive laser fusion, J. Fusion Energy **27**, 2531 (2007).

[29] F. J. Marshall and J. A. Oertel, A framed monochromatic x-ray microscope for ICF (invited), Rev. Sci. Instrum. **68**, 735 (1997).

[30] A. Bose, R. Betti, D. Shvarts, and K. M. Woo, The physics of long- and intermediate-wavelength asymmetries of the hot spot: Compression hydrodynamics and energetics, Phys. Plasmas **24**, 102704 (2017).

[31] A. Bose, R. Betti, D. Mangino *et al.*, Analysis of trends in experimental observables: Reconstruction of the implosion dynamics and implications for fusion yield extrapolation for direct-drive cryogenic targets on OMEGA, Phys. Plasmas **25**, 062701 (2018).

[32] A. Ciardi, S. V. Lebedev, A. Frank *et al.*, The evolution of magnetic tower jets in the laboratory, Phys. Plasmas **14**, 056501 (2007).

[33] J P Chittenden, S V Lebedev, C A Jennings, S. N. Bland, and A. Ciardi, X-ray generation mechanisms in three-dimensional simulations of wire array Z-pinches, Plasma Phys. Controlled Fusion **46**, B457 (2004).

[34] C. A. Walsh, J. P. Chittenden, K. McGlinchey, N. P. L. Niasse, and B. D. Appelbe, Self-Generated Magnetic Fields in the Stagnation Phase of Indirect-Drive Implosions on the National Ignition Facility, Phys. Rev. Lett. **118**, 155001 (2017).

[35] J. D. Sadler, C. A. Walsh, and H. Li, Symmetric Set of Transport Coefficients for Collisional Magnetized Plasma, Phys. Rev. Lett. **126**, 075001 (2021).

[36] J. R. Davies, H. Wen, Jeong-Young Ji, and E. D. Held, Transport coefficients for magnetic-field evolution in inviscid magnetohydrodynamics, Phys. Plasmas **28**, 012305 (2021).

[37] C. A. Walsh, J. D. Sadler, and J. R. Davies, Updated magnetized transport coefficients: Impact on laser-plasmas with self-generated or applied magnetic fields, Nucl. Fusion **61**, 116025 (2021).

[38] C. A. Walsh, R. Florido, M. Bailly-Grandvaux *et al.*, Exploring extreme magnetization phenomena in directly driven imploding cylindrical targets, Plasma Phys. Controlled Fusion **64**, 025007 (2022).

[39] L. Spitzer, Jr. and R. Harm, Transport phenomena in a completely ionized gas, Phys. Rev. **89**, 977 (1953).

[40] M. R. Gomez, S. A. Slutz, A. B. Sefkow *et al.*, Experimental Demonstration of Fusion-Relevant Conditions in Magnetized Liner Inertial Fusion, Phys. Rev. Lett. **113**, 155003 (2014).

[41] P. F. Schmit, P. F. Knapp, S. B. Hansen *et al.*, Understanding Fuel Magnetization and Mix Using Secondary Nuclear Reactions in Magneto-Inertial Fusion, Phys. Rev. Lett. **113**, 155004 (2014).

[42] E. L. Vold, A. S. Joglekar, M. I. Ortega, R. Moll, D. Fenn, and K. Molvig, Plasma viscosity with mass transport in spherical inertial confinement fusion implosion simulations, Phys. Plasmas **22**, 112708 (2015).

[43] D. J. Bernstein, T. Lafleur, J. Daligault, and S. D. Baalrud, Friction force in strongly magnetized plasmas, Phys. Rev. E **102**, 041201(R) (2020).

[44] D. J. Bernstein and S. D. Baalrud, Effects of Coulomb coupling on friction in strongly magnetized plasmas, Phys. Plasmas **28**, 062101 (2021).